Journal of the Mechanical Behavior of Biomedical Materials 175 (2026) 107331

Contents lists available at ScienceDirect

Journal of the Mechanical Behavior of Biomedical Materials

journal homepage: www.elsevier.com/locate/jmbbm

Surface and microstructural properties of denture base materials: Effects of manufacturing techniques, surface treatments, and aging protocols

Laura Brose [a], Andreas Koenig [b], Paul Kemmesies [b], Saba Tamjidtash [c,d], Nadine Kommerein [c,d], Katharina Doll-Nikutta [c,d], Meike Stiesch [c,d], Martin Rosentritt [a], Sebastian Hahnel [a,*]

[a] Department of Prosthetic Dentistry, UKR University Hospital Regensburg, Germany
[b] Department of Dental Prosthetics and Materials Science, Leipzig University, Liebigstraße 12, 04103, Leipzig, Germany
[c] Department of Prosthetic Dentistry and Biomedical Materials Science, Hannover Medical School, Hannover, Germany
[d] Lower Saxony Centre for Biomedical Engineering, Implant Research and Development (NIFE), Hannover, Germany

ARTICLE INFO

Keywords:
Denture base material
Auto-curing
Milling
Three-dimensional printing
Artificial aging
Surface properties

ABSTRACT

Objectives: Understanding denture base material properties under aging conditions is crucial for assessing their clinical performance and impact on oral health. This study evaluated the behaviour of polymethylmethacrylate (PMMA), dimethacrylate-based polymers (DMA), and polyetheretherketone (PEEK) denture base materials after aging (thermal, mechanical, chemical), based on parameters (surface, mechanical, sorptive, structural) and considering manufacturing techniques (auto-curing, milling, 3D printing).

Material and methods: Disc-shaped specimens (2 mm × 8 mm, n = 10 per group; total n = 500) were manufactured from five denture base materials: PMMA (auto-curing, milling), DMA (3D printing: 90°/45° orientation), PEEK (milling). Standardized rough or fine surfaces were applied. Specimens underwent separate aging protocols: thermocycling, toothbrush abrasion, storage in HCl/NaOCl. Surface and material properties were analyzed prior and after aging. Data were evaluated using non-parametric tests (Kruskal-Wallis, Mann-Whitney U, $\alpha = 0.05$). Effect sizes were calculated.

Results: Compared to other materials, PEEK showed few significant changes in surface parameters, microhardness, and indentation after aging. All materials exhibited strong effect sizes for water absorption and solubility ($r \geq 0.85$***). In PMMA, aging significantly reduced surface and mechanical properties, especially in rough-treated specimens. DMA printed with 90° was less affected by aging than with 45°, particularly after fine treatment. Milled PMMA with fine treatment showed the highest aging resistance among PMMA variants. Generally, rough surfaces were more susceptible to aging than fine surfaces.

Conclusion: Aging resistance of denture base materials depends on surface treatment, material, and manufacturing technique. Adequate polishing reduces aging effects on surface and mechanical properties. Milling yields reliable results, while 3D printing requires further optimization.

1. Introduction

Removable dental prostheses (RDPs) are used to improve the state of health by restoring masticatory function, speech, and facial aesthetics in partially or completely edentulous patients (Gupta et al., 2019; Lee and Saponaro, 2019; Roessler, 2003). Currently, most RDPs are fabricated from polymethylmethacrylate (PMMA), which is an amorphous thermoplastic with long, disordered molecular chains, resulting in a transparent, hard, and brittle material at ambient conditions (Bargel and Schulze, 2008; Roos and Maile, 2015; Koltzenburg et al., 2024). Under mechanical stress, its macromolecules stretch and align until entanglements limit deformation, with entropic elasticity causing the material to revert to its initial state after unloading (Bargel and Schulze, 2008). Softening begins at temperatures higher than 60–80 °C and coincides with a significant loss of strength. It progresses with further heating to complete chain degradation (Roos and Maile, 2015; Koltzenburg et al., 2024). PMMA features favourable processability, low costs, moderate solubility, and acceptable toxicity, although polymerization shrinkage

* Corresponding author. Department of Prosthetic Dentistry, UKR University Hospital Regensburg, 93042, Regensburg, Germany.
E-mail address: sebastian.hahnel@ukr.de (S. Hahnel).

https://doi.org/10.1016/j.jmbbm.2025.107331
Received 3 October 2025; Received in revised form 2 December 2025; Accepted 29 December 2025
Available online 29 December 2025

can impair the fit of the dental prosthesis (Lee and Saponaro, 2019; Ribeiro et al., 2023; Tieh et al., 2022; Porwal et al., 2017; Lepišová et al., 2025).

In the recent years, polyetheretherketone (PEEK) has been introduced as an alternative material for the fabrication of RDPs. It is a semi-crystalline thermoplastic resin comprising ordered crystalline and disordered amorphous regions (Lepišová et al., 2025). Regularly arranged side groups promote crystallinity, strengthen intermolecular interactions and confer high mechanical strength as well as an opaque appearance (Bargel and Schulze, 2008; Roos and Maile, 2015). The amorphous domains work as flexible connecting segments, enhancing toughness and elasticity (Bargel and Schulze, 2008). Upon exceeding the glass transition temperature, amorphous areas become mobile while crystalline regions maintain their dimensional stability only at the crystalline melting point due to the ordered structures transition to the amorphous state (Bargel and Schulze, 2008). The degree of crystallinity, influenced by cooling rates, affects the elastic modulus and dimensional stability (Bargel and Schulze, 2008). PEEK also exhibits excellent chemical resistance, minimal water absorption, and superior thermal stability, making it particularly suitable for RDPs. (Lepišová et al., 2025; Le Bars et al., 2023).

In contrast to the thermoplastic materials PMMA and PEEK, dimethacrylate-based materials (DMA) are highly cross-linked thermosets (Bargel and Schulze, 2008; Roos and Maile, 2015; Rosentritt et al., 2018). The dense network prevents plastic deformation and results in excellent dimensional stability, even under thermal stress (Bargel and Schulze, 2008). Due to the absence of a defined softening or melting range, DMA polymers exhibit no pronounced glass transition and remain in a solid state up to their decomposition temperature (Bargel and Schulze, 2008; Roos and Maile, 2015). Compared to thermoplastics, they demonstrate greater thermal stability and resistance to deformation (Bargel and Schulze, 2008).

Traditional processing of PMMA in the dental laboratory includes auto- and heat-curing. In auto-polymerization, the addition of an initiator, typically benzoyl peroxide in powder form, to the monomer methyl methacrylate (MMA) triggers a radical chain reaction (Rosentritt et al., 2018). This reaction occurs at room temperature, forming a continuous polymer network. However, incorrect pre-dosing can increase residual monomer content, shrinkage, or reduce compactability, thereby impairing mechanical properties (Rosentritt et al., 2018). Manual mixing requires prompt handling due to rapid viscosity changes. Polymerization in water and under pressure reduces air entrapment and improves the degree of polymerization (Rosentritt et al., 2018). More modern approaches, such as injection molding, decrease polymerization shrinkage and maintain constant pressure during processing, but require more complex equipment and higher processing temperatures (Rosentritt et al., 2018).

With the introduction of computer-aided design (CAD) and computer-aided manufacturing (CAM), subtractive (milling) and additive (printing) manufacturing of PMMA and DMA-based RDPs have also become possible. These digital workflows are more time-efficient and require less manual steps (Dimitrova et al., 2024; Da Silva et al., 2023; Kurzendorfer et al., 2023; Lo Russo et al., 2024; Kattadiyil et al., 2015; Nagar et al., 2024). In a subtractive production process, the RDPs are milled from an industrially pre-polymerized PMMA blank by sequential material removal with milling tools differing in granularity (Kurzendorfer et al., 2023). As the blanks are industrially polymerized under high pressure and temperature, shrinkage, microporosity, and residual monomer content are reduced (Tieh et al., 2022; Dimitrova et al., 2024; Wang et al., 2021).

Additive manufacturing techniques for RDPs include stereolithography and digital light processing (DLP) (Da Silva et al., 2023), in which a liquid denture base resin is selectively polymerized layer by layer. The RDPs are subsequently cleaned with isopropanol to remove residual unpolymerized resin, followed by post-curing under a specific wavelength to complete polymerization. In additive manufacturing processes, the built orientation can be individually selected, although a 90° angle is the most commonly used setting. With regard to this aspect, it is currently discussed whether the built orientation has an impact on the surface quality and mechanical properties of the printed object (Shim et al., 2020; Li et al., 2023).

Regarding the longevity of RDPs, several authors recommend replacement intervals ranging from five to ten years (Roessler, 2003; Taylor et al., 2021; Schwass et al., 2013; Khangura et al., 2023). In practice, however, RDPs are often used for considerably longer periods and there is limited conventional wisdom regarding an average longevity for RDPs (Taylor et al., 2021; Schwass et al., 2013). This phenomenon may be due to different materials and manufacturing techniques as well as individual patterns of use. With regard to this aspect, it is important to consider that in the oral cavity RDPs are continuously exposed to thermal fluctuations as well as mechanical and chemical stresses that foster aging of the materials. RDPs also provide vast interfaces for biofilm formation (Porwal et al., 2017; Abuhajar et al., 2023; Gendreau and Loewy, 2011; Ozyilmaz and Akin, 2019; Hahnel et al., 2009; Muscat et al., 2018), which is why regular mechanical and chemical cleaning is recommended (Schmutzler et al., 2021). Both mechanical and chemical cleaning of RDPs may affect surface and mechanical properties (Ribeiro et al., 2023; Porwal et al., 2017; Ozyilmaz and Akin, 2019).

The introduction of subtractive and additive manufacturing techniques employing novel PMMA-, DMA- or PEEK-based materials raises the question whether the surface and material properties are improved in relation to conventionally applied materials for the fabrication of RDPs.

Against this background, the aim of the current study was to evaluate the behaviour of differently produced PMMA, DMA, and PEEK surfaces against various simulated thermal, mechanical, and chemical aging protocols. In case of PMMA and DMA, it was also investigated in how far the manufacturing technique (auto-curing, milling, or printing) affects aging behaviour. Based on these objectives, the following research hypotheses were formulated:

I. PEEK exhibits superior surface and mechanical properties and is less affected by artificial aging compared to PMMA or DMA.
II. The fabrication technique (auto-curing, milling, printing) has a significant effect on the surface and mechanical properties of artificially aged PMMA and DMA.
III. Milled PMMA is less susceptible to deterioration of surface and mechanical properties caused by artificial aging than auto-cured PMMA or printed DMA.

2. Materials and methods

2.1. Study design

Fig. 1 illustrates the study design and the number of analyzed specimens. Five denture base resins were investigated, processed by distinct manufacturing protocols: PMMA via reactive polymerization (PMMA-C) and milling (PMMA-M), DMA via 3D printing with build orientations of 90° (DMA90-P) and 45° (DMA45-P), and PEEK via milling (PEEK-M). For each material, two surface finish variants (rough (A) and fine (B)) were prepared. Specimens were subjected to four aging protocols: thermocycling (TC), toothbrush abrasion (TBA), and storage in hydrochloric acid (HCl) or sodium hypochlorite (NaOCl). Non-aged specimens served as references. All specimens were produced as cylindrical discs with a thickness of 2 mm and a diameter of 8 mm. For each material-surface-aging combination, $n = 10$ specimens were prepared, resulting in a total of $n = 500$. Surface and material properties were comprehensively characterized. For phase composition analysis by X-ray diffractometry, only non-aged specimens were examined. In addition, surface treatment was not considered in the X-ray diffractometry, differential scanning calorimetry, or thermogravimetric analysis.

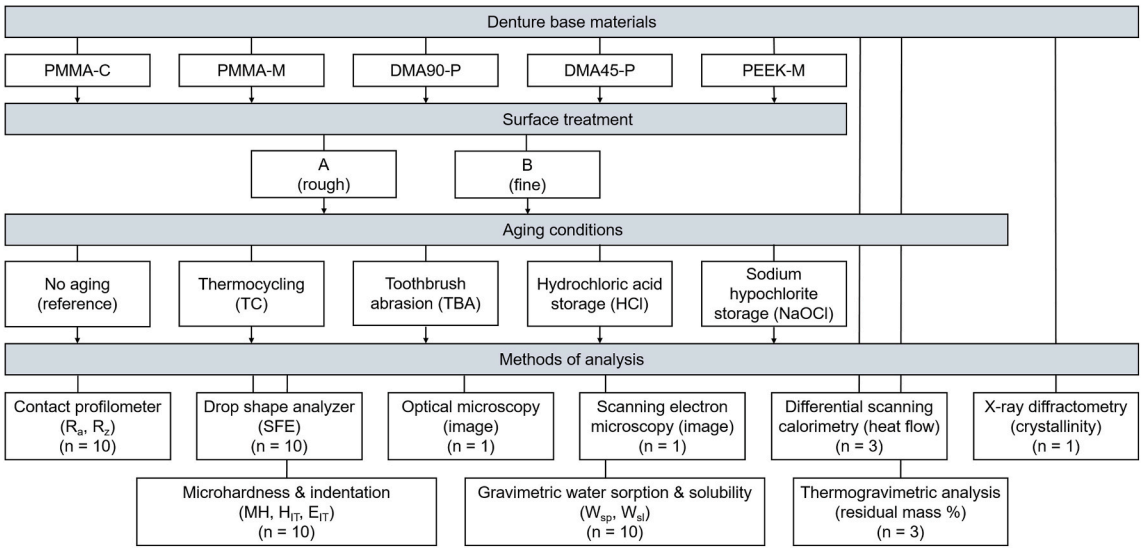

Fig. 1. An overview of the study design and the number of specimens (PMMA-C: PMMA by conventional auto-curing, PMMA-M: PMMA by milling, DMA90-P: DMA by 90° built orientation and printing, DMA45-P: DMA 45° by built orientation and printing, PEEK-M: PEEK by milling).

2.2. Materials

Five denture base materials processed by distinct manufacturing methods were investigated (Table 1):

2.2.1. Auto-curing

Cold-polymerized PMMA-C specimens were produced by mixing powder (5 g) and liquid components (3.5 ml). After powder addition, the suspension was stirred for approximately 15 s under bubble-free conditions. The resulting homogeneous mixture was cast into metal molds and planarized with glass plates. Polymerization was carried out in water (55 °C) using a pressure pot with a pressure of 2 bar for 20 min.

2.2.2. Milling

PMMA-M and PEEK-M were vertically oriented within the digital blank using the inLab CAM SW 22 (version: 22.6.1.282805, Dentsply Sirona, Bensheim, Germany) and machined wet on a five-axis milling unit (inLab MC X5, Dentsply Sirona, Bensheim, Germany). Following milling, specimens were separated from the blanks using a handheld rotary instrument.

2.2.3. Printing

DMA90-P and DMA45-P were produced by digital light processing (DLP, P30+, Straumann, Freiburg, Germany). Specimens were built at 90° and 45° orientations relative to the build platform with a layer thickness of 50 µm. Each layer was polymerized by a light source. After printing, the specimens were cleaned of unpolymerized material using 99.8 % isopropanol (pure 2-Propanol, Walter CMP, Kiel, Germany) in an automated cleaning unit (P wash, Straumann, Freiburg, Germany) (Table 2). After a waiting period of 15 min, final polymerization was carried out in a post-curing unit (P cure, Straumann, Freiburg, Germany). Support structures were then manually removed.

Table 2
Details of the two post-processing processes.

Unit	Program
P wash	pre-cleaning: 3:10 min cleaning: 2:10 min drying: 1:30 min
P cure	vacuum: 2:20 min curing: 10 min pressure compensation: 0:30 min

2.3. Surface treatment

All specimens were randomly assigned to one of two standardized surface treatments to produce uniform rough (A) or fine (B) topographies. Each specimen was mounted in holders and processed with an automated precision polishing unit (Tegramin-25, Struers, Willich, Germany) with defined setting parameters (Table 3). The parameters for the surface treatments were optimized in preliminary experiments to achieve the targeted line roughness values of approximately $R_a \approx 0.2$ µm for surface treatment A and $R_a \approx 0.04$ µm for surface treatment B. To eliminate potential surface influences from prior manufacturing processes and to ensure a homogeneous fine finishing, surface treatment B was carried out in two sequential processing steps.

2.4. Artificial aging protocols

The specimens were then randomly forwarded to one of four distinct artificial aging procedures. The aging protocols each simulated a one-year period of use.

2.4.1. Thermal aging – thermocycling (TC)

The specimens were placed in fine-mesh fabric bags to prevent

Table 1
Overview of the used denture base materials.

Material	Abbreviation	Manufacturing process	LOT number	Manufacturer
Palapress	PMMA-C	Conventional auto-curing	Powder: M010135 Liquid: M010139	Kulzer, Hanau, Germany
CediTEC DB	PMMA-M	Milling	2127008; 2331042	Voco, Cuxhaven, Germany
V-Print dentbase	DMA90-P	Printing, 90° orientation	2311630	Voco, Cuxhaven, Germany
V-Print dentbase	DMA45-P	Printing, 45° orientation	2311630	Voco, Cuxhaven, Germany
PEEK BioSolution	PEEK-M	Milling	13922; 22223	Merz Dental, Lütjenburg, Germany

Table 3
Settings for the surface treatment processes.

Treatment	Parameters	
Surface treatment A	Contact force	5 N (PMMA and DMA) 10 N (PEEK)
	Processing time	20 s
	Rotation speed (specimen holder and table)	150 rpm
	SiC-foil	grit of 1200 (Struers, Willich, Germany)
Surface treatment B	Contact force	5 N (PMMA and DMA) 10 N (PEEK)
	Processing time	20 s
	Rotation speed (specimen holder and table)	150 rpm
	SiC-foil	grit of 1200 (Struers, Willich, Germany)
	Followed by	
	Contact force	5 N (PMMA and DMA) 10 N (PEEK)
	Processing time	20 s
	Rotation speed (specimen holder and table)	120 rpm
	SiC-foil	grit of 4000 (Buehler, Dusseldorf, Germany)

floating during TC. They were then inserted into a thermocycler (Regensburger Kausimulator, eGo-Kältetechnik, Regensburg, Germany). Thermocycling was performed between 5 °C and 55 °C for a total of 10,000 cycles, simulating approximately one year of clinical use for removable dentures. Each cycle consisted of a 30 s dwell time at each temperature and a 30 s transfer time.

2.4.2. Mechanical aging – toothbrush abrasion (TBA)

Mechanical aging was simulated using a toothbrush simulator (ZM-3, SD Mechatronik, Feldkirchen-Westerham, Germany) to replicate daily brushing-induced wear. Toothbrush heads (Plu°line, dental bauer, Tuebingen, Germany) performed circular motions (8 mm diameter) at a speed of 40 mm/s under a constant load of 200 g. Each specimen was subjected to 7200 brushing cycles. During testing, specimens were covered with 10 ml of a slurry consisting of 250 g toothpaste (Colgate Total Original, CP GABA, Hamburg, Germany) mixed with 1 l deionized water.

2.4.3. Chemical aging – hydrochloric acid (HCl)

To simulate gastric acid exposure under reflux conditions, specimens were immersed in a hydrochloric acid solution adjusted to pH ≈ 1.52. The solution was prepared by diluting concentrated HCl (37 %, Merck, Darmstadt, Germany) with deionized water in a 1:4 ratio. The target pH was confirmed using a calibrated pH meter (Type 764, Knick Elektronische Messgeräte, Berlin, Germany). Specimens were stored in sealed containers and incubated at 37 °C (B6, Heraeus, Hanau, Germany) for 7 d.

2.4.4. Chemical aging – sodium hypochlorite (NaOCl)

For chemical aging, specimens were stored in 30 ml of a 1 % sodium hypochlorite solution (Histolith NaOCl 1 %, lege artis Pharma, Dettenhausen, Germany) at 37 °C for 60 h and 50 min in an incubator (B6, Heraeus, Hanau, Germany). This duration corresponds to one year of simulated clinical use, assuming daily exposure of 10 min.

Following artificial aging, all specimens were steam-cleaned and dried using a lint-free tissue.

2.5. Material characterization

2.5.1. Surface analyses

Surface roughness was analyzed using a contact profilometer (Perthometer S6P, Perthen Mahr, Goettingen, Germany). The measurement parameters were set as follows: LT = 1.7 mm/0.25 mm, horizontal and vertical interval = 50 µm, z-resolution = 0.5 µm, and x-resolution = 1 µm. The line roughness parameters arithmetical mean roughness (R_a, in µm) and average roughness depth (R_z, in µm) were evaluated as two-dimensional surface roughness descriptors. To ensure standardized measurement conditions, the specimens were oriented in a way that the macroscopic polishing marks were aligned orthogonally to the scan direction. Roughness measurements were performed at the centre of the specimen surface using a diamond stylus with a tip radius of 2 µm and a scanning speed of 0.1 mm/s.

The surface free energy (SFE, in mJ/m^2) was determined from contact angle measurements using an automated contact angle measuring instrument (Drop Shape Analyzer DSA25, Krüss, Hamburg, Germany), following the guidelines of ISO 19403–2:2024. Prior to the measurements, the specimens were cleaned with 70 % ethanol and allowed to air dry. Using the sessile drop method, 1 µL droplets of deionized water and diiodomethane were analyzed at a room temperature of approximately 23 °C. The SFE was then calculated using the Owens and Wendt method (Owens and Wendt, 1969).

For visual examination, one specimen per group was randomly selected to capture the surface topography. To provide an overview, initial images were acquired using an optical microscope (lens type: ZS20, VHX-S550E, Keyence, Osaka, Japan) at a magnification of 30 × . Scanning electron microscopy (SEM, Phenom, FEI, The Netherlands) was additionally performed with a magnification of 1500 × and a working distance of 160 µm. For SEM analyses, specimens were mounted on aluminium stubs and sputter-coated with a thin layer of platinum for 50 s to prevent electrostatic charging and to enhance image quality.

2.5.2. Microhardness and indentation

Hardness parameters were determined immediately after aging using a universal hardness testing machine (ZwickiLine Z2.5, ZwickRoell, Ulm, Germany) in accordance with DIN EN ISO 14577-1. A Vickers indenter was employed to provide a constant loading rate of 0.1 mm/min and a maximum force of 30 N. The peak force was maintained for a duration of 2 s. The following parameters were evaluated: Martens hardness (HM, in N/mm^2), indentation hardness (H_{IT}, in N/mm^2), and indentation modulus (E_{IT}, in kN/mm^2).

2.5.3. Gravimetric determination of water absorption and solubility

To characterize the water-related behaviour of the materials, water sorption (W_{sp}, in $µg/mm^3$) and solubility (W_{sl}, in $µg/mm^3$) were evaluated. The volume of each specimen was first calculated by measuring thickness and diameter. The specimens were then placed on a perforated tray inside a desiccator with silica gel (Silica Gel Orange, Carl Roth, Karlsruhe, Germany) at the bottom, and the desiccator was stored in an incubator (B6, Heraeus, Hanau, Germany). W_{sp} and W_{sl} were finally determined in accordance with DIN EN ISO 10477:2021–02.

2.5.4. Structural analyses

The phase composition of the unaged polymer-based specimens was characterized using X-ray diffraction (XRD). A MINIFLEX 600 (Rigaku, Tokyo, Japan) with Cu Kα radiation (1.5418 Å, 40 kV 10 mA) and a DTex Ultra 2 MF detector (Rigaku, Tokyo, Japan) was used. The monolithic specimens were measured with a diffraction angle between 10 and 140° on a Si single crystal plate to minimize the influence of the background. The measurement data was evaluated using search-match analysis and partial Rietveld analysis with SMARTLAB Studio II v5.0.174.0 software (Rigaku, Tokyo, Japan) and data stems from the PDF5 the database (ICDD. Newtown Square, USA). An error of 1–2 % by mass was assumed for the weight percentages, because of the higher R_{wp}-values (Jansen et al., 2011).

Differential scanning calorimetry (DSC) was performed using a DSC 204 F1 Phoenix instrument (NETZSCH, Selb, Germany). Measurements (n = 3 per material and aging condition) were conducted within temperature ranges of 35–250 °C and 35–400 °C at a heating rate of 20 K/

min under a nitrogen atmosphere. Specimens with a mass of approximately 5 mg were placed in aluminium crucibles for analysis. The data were analyzed using the Proteus Analysis software (version 6.1.0).

Thermogravimetric analysis (TGA) was performed using a TG 209 F3 Tarsus instrument (NETZSCH, Selb, Germany). The specimens were placed in open Al_2O_3 crucibles (70 µl, ME-24123, Mettler-Toledo, Vienna, Austria). Initially, the empty crucibles were weighed, followed by weighing of the crucibles containing the specimens (approximately 11 mg, crushed; n = 3 per material and aging condition). Subsequently, the specimens were subjected to a heating program within a temperature range of 25–600 °C or 25–900 °C, respectively, at a heating rate of 20 K/min under a nitrogen atmosphere. During heating, the specimens continuously lost mass until thermal decomposition of the material was completed. The residual material was determined gravimetrically and expressed as the residual mass fraction (in %). The Proteus Analysis software (version 6.1.0) was used to evaluate the data.

2.6. Statistics

All statistical analyses were performed using SPSS Statistics 29 (IBM Corp., Armonk, NY, USA). Data of the surface analyses, microhardness and indentation, as well as water absorption and solubility, were statistically evaluated using the Shapiro-Wilk test for normality and the Levene's test for homogeneity of variances. Based on these results, non-parametric analysis were performed using the Kruskal-Wallis test, followed by pairwise comparisons with the Mann-Whitney *U* test where appropriate. Statistical significance was defined as follows: $p > 0.05$ = not significant (n.s.); $p < 0.05$ = *; $p < 0.01$ = **; $p < 0.001$ = ***. Effect sizes (r) were calculated to evaluate the magnitude of significant differences. The significance level was set at $\alpha = 0.05$.

3. Results

Normal distribution could be assumed for 83 % of the tested groups (Shapiro-Wilk, $p > 0.05$) and homogeneity of variances was identified in 63 % of the tested groups (Levene). Effect sizes are expressed as r; asterisks indicate levels of statistical significance to the group without aging.

3.1. Surface analyses

3.1.1. Arithmetical mean roughness – R_a

Median R_a values (Fig. 2a) for specimens with treatment A ranged between 0.17 and 0.21 µm in the unaged condition, and ranged between 0.10 and 0.27 µm after aging. TC and HCl induced highest R_a, particularly in printed specimens (DMA90-P and DMA45-P). TBA exerted a significant smoothing effect across all materials ($p \leq 0.002$). Overall, the materials PMMA-M (TC: $r \geq 0.74$**; TBA: $r \geq 0.84$***; HCl: $r \geq 0.62$**; NaOCl: $r \geq 0.52$*) and DMA90-P (HCl: $r \geq 0.64$**; NaOCl: $r \geq 0.53$*) exhibited the most pronounced significant influences over the aging periods.

The fine treatment (B) resulted in consistently low R_a values (0.04–0.06 µm) in the unaged state. Across all aging protocols, R_a remained below 0.08 µm, reflecting reduced sensitivity compared to treatment A. TBA induced a significant decrease in R_a values in PMMA-C ($r \geq 0.78$***), DMA90-P ($r \geq 0.71$**) and PEEK-M ($r \geq 0.52$*). For all materials except PMMA-M, aging generally led to slight increases in surface roughness. PMMA-M showed no significant changes, with only a minimal roughness increase after NaOCl exposure. PEEK-M showed stable roughness values across aging protocols and showed only significant changes at TBA ($r \geq 0.01$**).

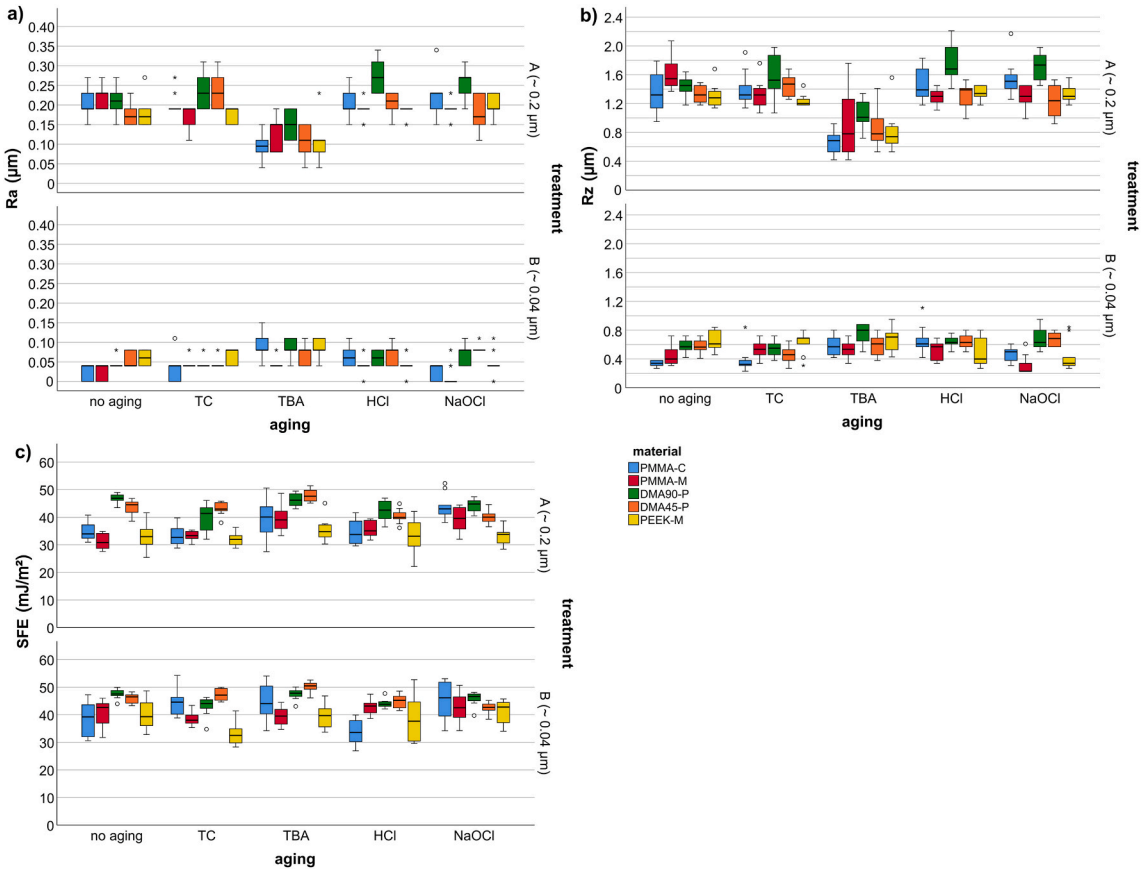

Fig. 2. Boxplots showing the distribution of surface analyses parameters in the tested materials following artificial aging processes. Circles denote mild outliers (>1.5 × interquartile range), while asterisks indicate extreme outliers (>3 × interquartile range). (a) R_a (median, µm). (b) R_z (median, µm). (c) SFE (median, mJ/m^2).

3.1.2. Average roughness depth – R_z

R_z values followed a trend similar to R_a (Fig. 2b). After treatment A, median R_z ranged from 1.3 to 1.6 µm in the unaged condition, with increased after TC, HCl, and NaOCl exposure, particularly in DMA90-P. In all materials, TBA led to a highly significant reduction in R_z (PMMA-C: r ≥ 0.85***; PMMA-M: r ≥ 0.67**; DMA90-P: r ≥ 0.01***; DMA45-P: r ≥ 0.01***; PEEK-M: r ≥ 0.01**). PMMA-M (TC: r ≥ 0.64**; TBA: r ≥ 0.67**; HCl: r ≥ 0.79***; NaOCl: r ≥ 0.72***) and DMA90-P (TBA: r ≥ 0,00***; HCl: r ≥ 0,61**; NaOCl: r ≥ 0,64**) showed the most significant changes. For PMMA-C, PMMA-M, and PEEK-M almost no significant differences were observed.

Fine treatment (B) resulted in consistently lower R_z (0.3–0.6 µm unaged; 0.2–0.8 µm after aging). TBA (PMMA-C: r ≥ 0.85***; DMA90-P: r ≥ 0.60**) induced moderate changes in R_z, whereas NaOCl led to highly significant variability in surface roughness (PMMA-C: r ≥ 0.63**; PMMA-M: r ≥ 0.57*; DMA45-P: r ≥ 0.49*; PEEK-M: r ≥ 0.57**).

3.1.3. Surface free energy – SFE

After treatment A, the median SFE values of the unaged specimens ranged from 31 to 47 mJ/m^2 (Fig. 2c). TBA led to significantly higher SFE medians in PMMA-M (r ≥ 0.76***) and DMA45-P (r ≥ 0.01***). In most cases, HCl and NaOCl significantly reduced SFE in DMA90-P (HCl: r ≥ 0.66**; NaOCl: r ≥ 0.57**), and DMA45-P (HCl: r ≥ 0.56*; NaOCl: r ≥ 0.59**), whereas PMMA-C (NaOCl: r ≥ 0.78***) and PMMA-M (HCl: r ≥ 0.61**; NaOCl: r ≥ 0.78***) showed partial increases. In general, PMMA-M, DMA90-P and DMA45-P exhibited the most significant changes in SFE compared to PMMA-C and PEEK-M.

Fine treatment (B) resulted in comparable or slightly higher SFE values relative to treatment A. TC produced the most significant changes in SFE for some materials (PMMA-C: r ≥ 0.47*; DMA90-P: r ≥ 0.73**; PEEK-M: r ≥ 0.62**), while PMMA-M and PEEK-M showed no significant changes under most conditions.

3.1.4. Visual recordings

Figs. 3 and 4 showed overview and detail images of the polished and aged specimens. Unaged specimens exhibited a consistent surface topography in specimens recorded with the optical microscope. Rough polishing produced matte surfaces, while fine polishing resulted in a glossy appearance with characteristic grinding marks. After TC and chemical aging, surfaces remained largely homogeneous. In contrast, mechanical aging by TBA caused pronounced grooves and localized indentations. DMA90-P and PEEK-M showed the least abrasion from brushing.

In the SEM images, the rough-polished specimens exhibited a pronounced polishing pattern, whereas the fine-polished specimens showed fewer polishing lines and a homogeneous surface texture. TBA was characterized by the absence of visible polishing lines in the rough treatment.

3.2. Microhardness and indentation

3.2.1. Martens hardness – HM

Regarding HM (Fig. 5a), TC caused a reduction after surface treatment A, particularly in PMMA-C (r ≥ 0.83***; decrease from unaged 128 N/mm^2 to 84 N/mm^2) and PMMA-M (r ≥ 0.58**). TBA (PMMA-M: r ≥ 0.85***), HCl (PMMA-C: r ≥ 0.68**; PEEK-M: r ≥ 0.66**), and NaOCl (PMMA-M: r ≥ 0.83***) produced fewer significant differences for all materials. No significant changes were identified for DMA90-P and DMA45-P after artificial aging.

For specimens with fine surface treatment (B), similar or slightly reduced HM values were identified in relation to those with treatment A, although a similar trend across all aging protocols was observed.

3.2.2. Indentation hardness – H_{IT}

For H_{IT} (Fig. 5b) and for specimens with surface treatment A, TC significantly reduced H_{IT}, particularly in PMMA-C (r ≥ 0.79***) and PMMA-M (r ≥ 0.52*). Chemical aging also had significant effects on PMMA-M (NaOCl: r ≥ 0.67**) and PEEK-M (HCl: r ≥ 0.72**). PEEK-M showed the highest median H_{IT} values across all conditions (approx. 279–315 N/mm^2) with only little variation between aging protocols. In contrast, PMMA-M showed the lowest but stable values with limited scatter.

Treatment B resulted in similar or slightly reduced H_{IT} values in comparison to treatment A. Similar trends were observed across aging protocols, but more significant differences were observed in TC (PMMA-C: r ≥ 0.79***; PMMA-M: r ≥ 0.85***; DMA90-P: r ≥ 0.51*; DMA45-P: r ≥ 0.63**) and HCl (PMMA-M: r ≥ 0.46*; DMA90-P: r ≥ 0.56*; DMA45-P: r ≥ 0.66**). PEEK-M (n.s.) featured superior hardness stability under all conditions.

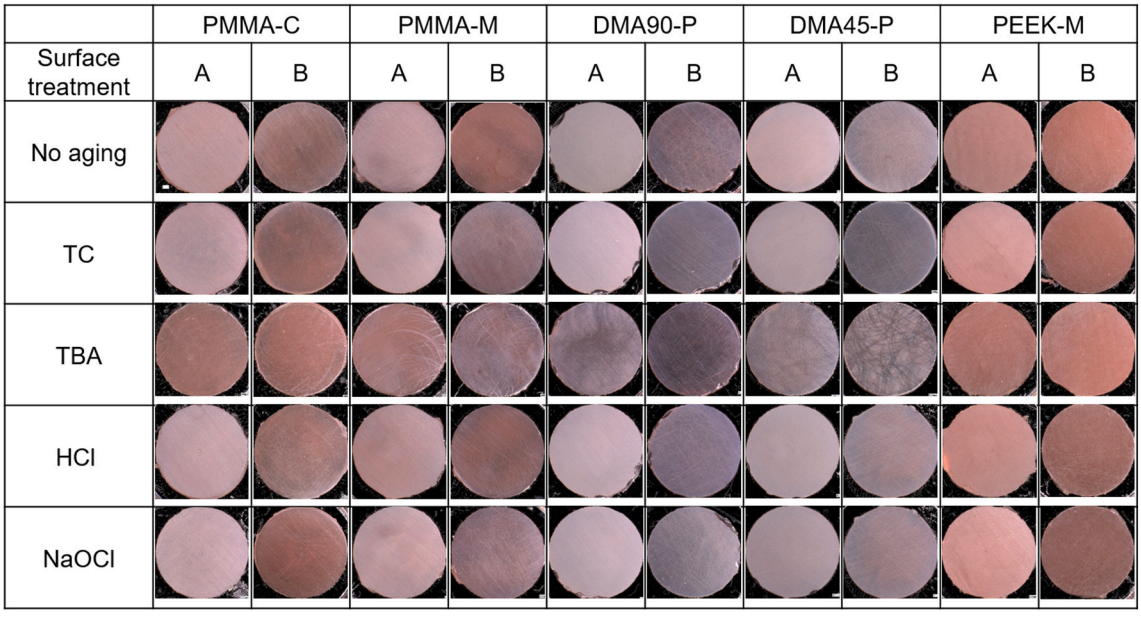

Fig. 3. Imaging of representative specimens to visualise the surface topography using an optical microscope (magnification: 30 × ; white bar: 500 µm for each image).

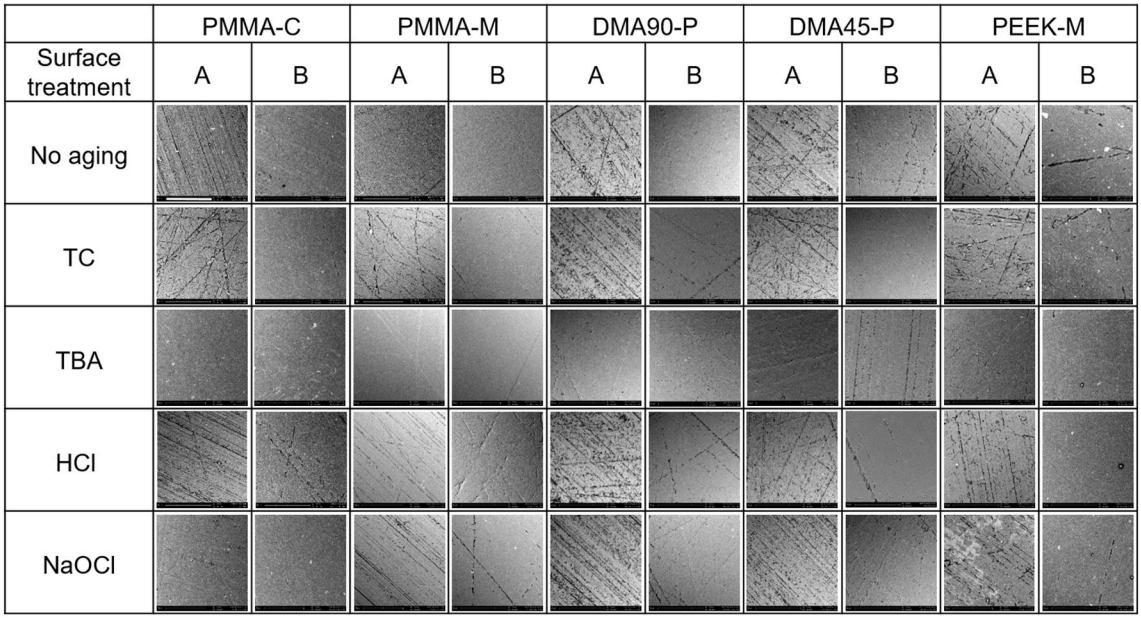

Fig. 4. Imaging of representative specimens to visualise the surface topography using a SEM (magnification: 1500 × ; white bar: 80 μm for each image).

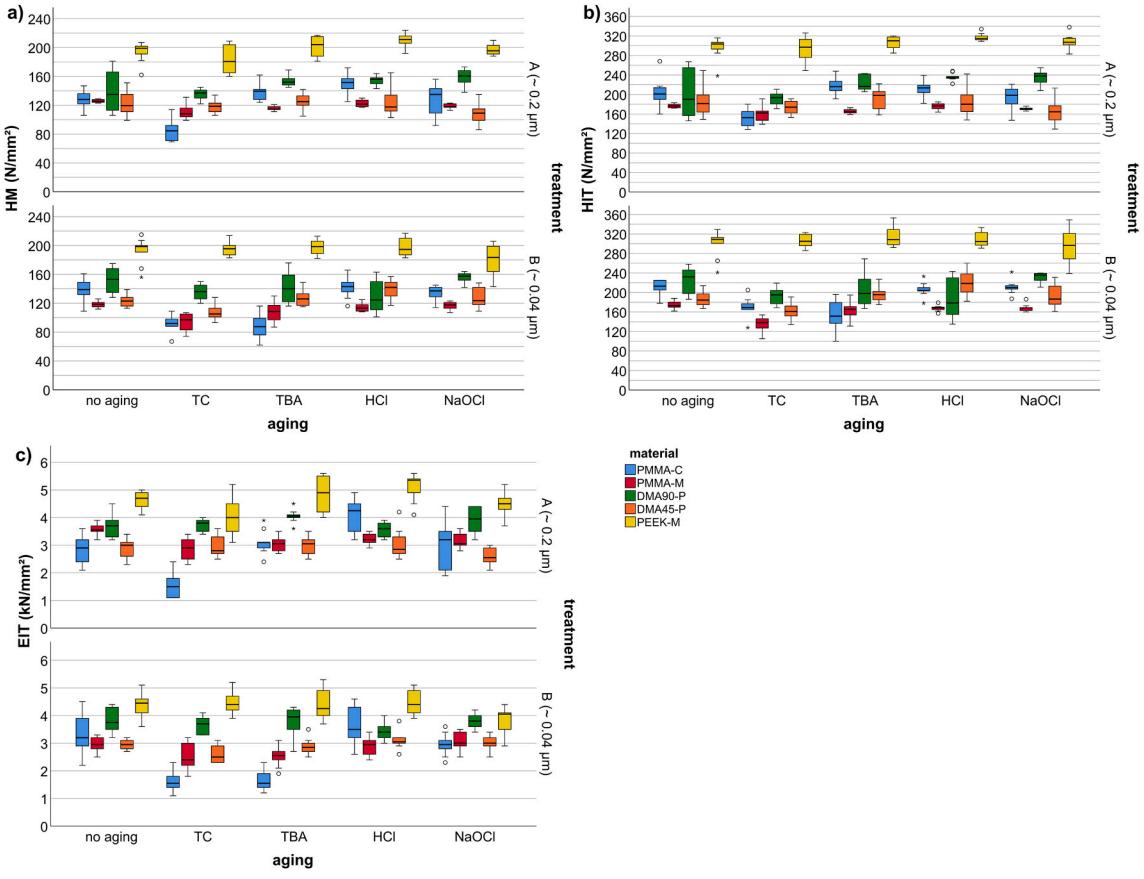

Fig. 5. Boxplots showing the distribution of hardness parameters of the tested materials after artificial aging processes. Circles denote mild outliers (>1.5 × interquartile range), while asterisks indicate extreme outliers (>3 × interquartile range). a) HM (median, N/mm^2). b) H_{IT} (median, N/mm^2). c) E_{IT} (median, kN/mm^2).

3.2.3. *Indentation modulus – E_{IT}*

For E_{IT} (Fig. 5c) and specimens after treatment A, TC led to a significant reduction in E_{IT} for PMMA-C ($r \geq 0.82$***), PMMA-M ($r \geq 0.79$***), and PEEK-M ($r \geq 0.50$*). Chemical aging significantly affected E_{IT} in PMMA-C (HCl: $r \geq 0.77$***), PMMA-M (HCl: $r \geq 0.67$**; NaOCl: $r \geq 0.70$**), and PEEK-M ($r \geq 0.53$*). TBA significantly reduced E_{IT} in PMMA-M ($r \geq 0.75$***).

Similar or slightly lower E_{IT} values were determined for the fine

treatment (B) in comparison to specimens subjected to treatment A, with fewer significant differences.

3.3. Gravimetric determination of water absorption and solubility

3.3.1. Water sorption – W_{sp}

For W_{sp} (Fig. 6a) and treatment A, TC resulted in increased W_{sp} for PMMA-M ($r \geq 0.85$***) as well as for DMA90-P (23.6 µg/mm^3; $r \geq 0.85$***), DMA45-P (23.8 µg/mm^3; $r \geq 0.85$***), and PEEK-M ($r \geq 0.84$***). PMMA-M (TBA: $r \geq 0.81$***; HCl: $r \geq 0.85$***; NaOCl: $r \geq 0.85$***) and DMA45-P (TBA: $r \geq 0.01$***; HCl: $r \geq 0.85$***; NaOCl: $r \geq 0.80$***) exhibited significant differences across all aging protocols. In contrast, PMMA-C showed no significant changes, while PEEK-M consistently showing lowest W_{sp} values.

Similar trends were identified for treatment B, with PEEK-M showing lowest W_{sp} (2.9–4.4 µg/mm^3) across all conditions. PMMA-C and DMA materials had higher values. For PMMA-M, significant differences were detected after TBA ($r \geq 0.64$***). DMA45-P ($r \geq 0.85$***) and DMA90-P showed significant increases in W_{sp} across most aging conditions. PEEK-M was significantly affected by the chemical agings (HCl: $r \geq 0.70$**; NaOCl: $r \geq 0.63$**).

3.3.2. Solubility – W_{sl}

For W_{sl} (Fig. 6b) and treatment A, TC, TBA, and HCl led to significant changes across all materials, with particularly strong effects for PMMA-M ($r \geq 0.85$***). For TBA, significant differences were detected, but with negligible effect sizes ($r \geq 0.01$***). NaOCl did not lead to any significant changes in PMMA-C and PEEK-M. TC resulted in increased W_{sl} in DMA90-P and DMA45-P, whereas the unaged condition exhibited negative median values for these materials (DMA90-P: 2.4 µg/mm^3; DMA45-P: 3.4 µg/mm^3). TBA significantly increased W_{sl} in the DMA materials ($p \leq 0.001$), while HCl exposure caused significantly divergent effects, with a decrease in DMA90-P ($p \leq 0.002$) and an increase in DMA45-P ($p \leq 0.001$).

For treatment B, similar trends were observed. With the exception of TBA in PMMA-C and PMMA-M, all aging protocols resulted in significant changes for all materials. TC again produced the highest W_{sl} values, whereas all other agings produced lower values. DMA45-P exhibited the highest number of significant increases with the strongest effect sizes ($r \geq 0.85$***). PEEK-M consistently showed the lowest W_{sl} across all conditions.

3.4. Structural analyses

3.4.1. Phase compositions

Unaged PMMA- (PMMA-C, PMMA-M) and unaged DMA- (DMA90-P, DMA45-P) based specimens exclusively showed broad X-ray amorphous areas, which indicated a low order state (similar to a glass) (Fig. 7a). Both the unaged PMMA and the unaged DMA-based materials were very similar to each other in the signal. Qualitative identification of the polymers was therefore possible. Individual sharp reflexes were detected in unaged PEEK-M specimens (Fig. 7b). Rutile (TiO_2) and semi-crystalline PEEK-M were detected qualitatively. Using the rietveld refinement, 2 % rutile (TiO_2) and a 31 % crystalline and 67 % X-ray amorphous proportion of PEEK ($C_{36}H_{22}O_4$) could be determined (Table 4). For this purpose, CaF_2 was added as a standard.

3.4.2. DSC

The heat flow measured by DSC revealed material-specific curve profiles, with aging having only minor effects (Fig. 8a–e). In PMMA-C, TC resulted in a flattened peak, while PMMA-M exhibited an additional, distinct peak at ~190 °C, which was absent under other aging conditions. For DMA90-P and DMA45-P, aging had minimal influence on heat flow behaviour. In contrast, the DSC profile of PEEK-M differed markedly from the other four denture base materials. Its DSC curves indicated a negligible impact of aging, consistently showing a prominent peak at ~340 °C across all conditions.

3.4.3. TGA

TGA revealed weight loss in all materials (Fig. 9a–e). PMMA-C and PMMA-M showed similar degradation profiles, with weight loss starting at ~220 °C (PMMA-C) and ~300 °C (PMMA-M) and reaching 0 % residual mass at ~420 °C, which indicates no inorganic content. DMA90-P and DMA45-P exhibited comparable behaviour, with degradation beginning at ~280 °C and ~200 °C, respectively, and residual masses ranging from 3.91 to 6.92 % (DMA90-P) and 2.40–6.04 % (DMA45-P). PEEK-M displayed a distinct profile: initial gradual weight loss, followed by a sharp drop between 550 and 600 °C, leaving a residual mass of 50.86–57.51 %. Aging had no significant effect on thermal degradation or weight loss in any material.

4. Discussion

The long-term performance and reliability of RDPs are significantly influenced by the aging resistance of the material and its interaction with clinical processing methods. Considering the clinical relevance of durable denture base materials in clinical dentistry, this study aimed to evaluate the resistance of PMMA, DMA, and PEEK processed with different manufacturing techniques to various types of artificial aging, including thermal, mechanical, and chemical stress. Within the limitations of the current study, the first research hypothesis suggesting that PEEK exhibits superior surface and mechanical properties and is less

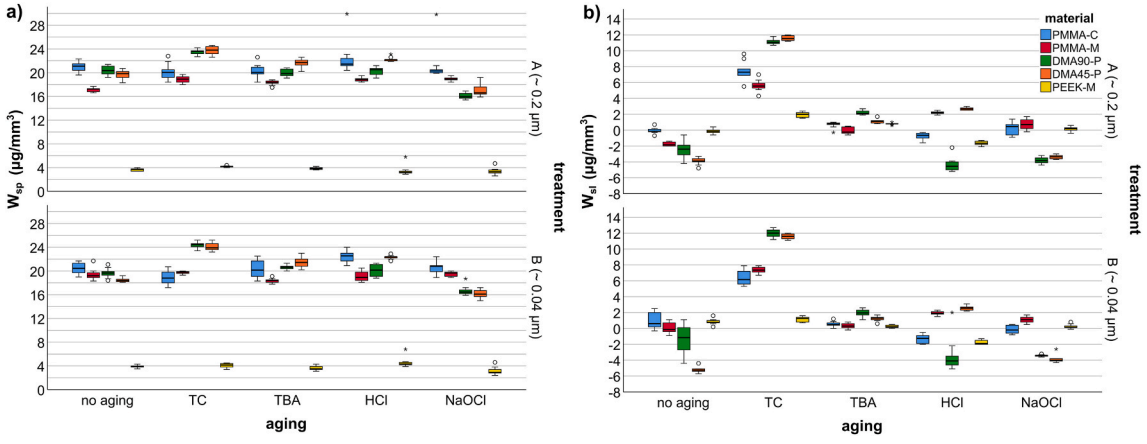

Fig. 6. Boxplots showing the distribution of water absorption and solubility parameters of the tested materials after artificial aging processes. Circles denote mild outliers (>1.5 × interquartile range), while asterisks indicate extreme outliers (>3 × interquartile range). a) W_{sp} (median, µg/mm^3). b) W_{sl} (median, µg/mm^3).

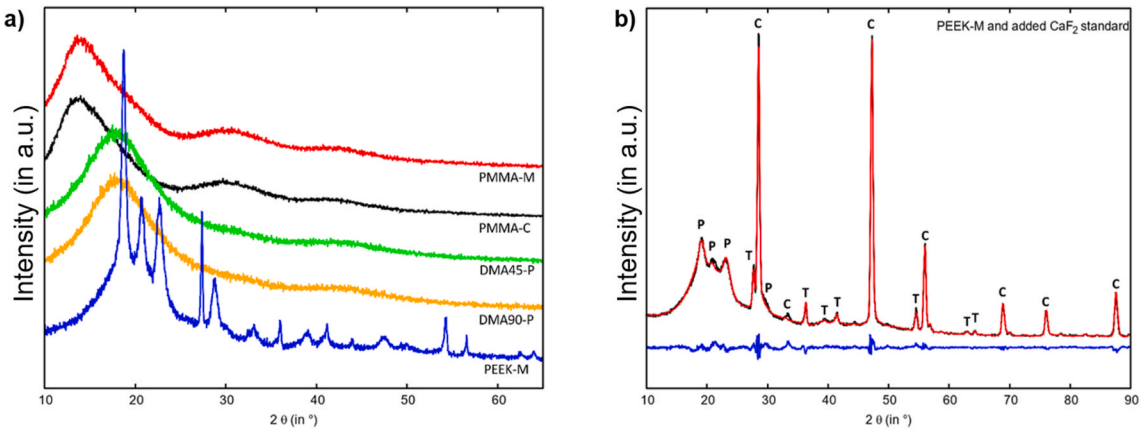

Fig. 7. Diffractograms of unaged analyzed specimens. a) Powder X-ray diffractogram of the unaged specimen PMMA-C, PMMA-M, DMA90-P and DMA45-P. b) Powder X-ray diffractogram of the unaged specimen PEEK-M. The measured curve is shown in black, the calculated curve in red. The difference between the two is shown in blue. All reflexes could be assigned and were labeled with letters. P stands for the crystalline part of the organic PEEK-M compound, T for TiO_2 (rutile crystal structure) and C for the added standard CaF_2 (fluorite crystal structure). (For interpretation of the references to colour in this figure legend, the reader is referred to the Web version of this article.)

Table 4
Parameters of rietveld analysis of PEEK-M. R_{wp}: weighted profile R-factor; R_{wp}: profile R-factor; S: goodness-of-fit; X^2: chi-squared statistic.

Parameter	Flourite	Rutile	Crystallized PEEK	X-ray-armorphic portion
R_{wp}	4.15			
R_p	3.18			
S	1.7223			
X^2	2.9663			
Weight percentages	(0.0) excluded	2.38(7)	30.5(3)	67.1(3)
Space group/ number	Fm $\bar{3}$ m; 225	$P4_2/mnm$; 136	$P2_1/b$; 14	
PDF-Nr.:	04-009-5311	01-088-6627	20867496 (ICDD)	–
lattice parameters				
a in Å	5.46945	4.59677	7.76591	–
b in Å	5.46945	4.59677	6.01304	–
c in Å	5.46945	2.96177	26.42036	–
α in °	90.000	90.000	96.273	–
β in °	90.000	90.000	90.000	–
γ in °	90.000	90.000	90.000	–
Lattice volume in $Å^3$	163.618	62.583	1226.355	–

affected by artificial aging compared to PMMA or DMA could be confirmed. The second hypothesis suggesting that the fabrication technique (auto-curing, milling, printing) has a significant effect on the surface and mechanical properties of artificially aged PMMA and DMA could only be partially confirmed. Moreover, the third research hypothesis implying that milled PMMA is less susceptible to deterioration of surface and mechanical properties caused by artificial aging than auto-cured PMMA or printed DMA was also only partially accepted.

4.1. Surface analyses

4.1.1. Roughness

As expected, the different initial surface treatments (rough and fine) produced different surface roughness values R_a and R_z. TC and HCl aging increased R_a, especially in printed specimens, while TBA significantly reduced R_a across all materials with rough surface. Fine treatment consistently produced low R_a values (<0.08 μm) and reduced sensitivity to artificial aging. PMMA-M featured the highest aging resistance, while DMA90-P also achieved outstanding results in the group with the fine polishing process. PEEK-M showed a slight but significant increase in roughness due to TBA (Brinkmann et al., 2025).

These findings align with previous literature. TC aging has been shown to increase surface roughness in printed materials (Zhang et al., 2024), though another study identified no significant effect of TC on R_a (Hahnel et al., 2009). In CAD/CAM resin composites, HCl storage significantly altered surface topography (S_a) (Schmohl et al., 2022). Similarly, NaOCl led to increased roughness in the present study, consistent with earlier results (Porwal et al., 2017). Conversely, a study with PEEK reported decreased roughness after 24 h of water storage, suggesting material-specific differences in aging responses (Babaier et al., 2022).

In line with Zhang et al. (2024), printed materials exhibited rougher surfaces and reduced hydrophilicity due to increased S_a and contact angle values compared to conventional and milled materials. This indicates that additional surface treatment or the application of a protective coating may be required prior to clinical use to enhance the mechanical performance (Dai et al., 2022). Zhang also noted a correlation between printing orientation and roughness, although it remained unclear which orientation would be optimal and whether post-processing was performed (Atalay et al., 2021). In the present study, a significant increase in R_a after TC aging was observed only at a 45° printing angle, but not with a 90° printing angle and for fine surface treatment. These results are contrary to earlier results by Gad et al., who observed increased roughness after TC in 90° printed DMA (Gad et al., 2022a).

Our data also revealed that DMA materials exhibited the most pronounced roughness changes in dependence of artificial aging. This phenomenon may be attributed to their high water absorption after TC, which can cause swelling and micro crack formation, ultimately increasing surface roughness. R_z, which captures peak-to-valley distances, is especially sensitive to such microdefects and may explain the increased variability observed. The higher instability of additively manufactured DMA compared to milled PMMA may also relate to the production methods: milled PMMA is polymerized under high pressure and temperature, resulting in lower residual monomer content and higher density. In contrast, printed DMA's layer-by-layer structure may introduce voids and leave higher monomer levels, making it more prone to degradation (Zhang et al., 2024).

Surface roughness measurement with a tactile contact profilometer is widely used in the literature (Mínguez-Martínez et al., 2022; Jones et al., 2004; Atalay et al., 2021; Liebermann et al., 2016), but it has several limitations. The instrument records only two-dimensional parameters such as R_a and R_z (Rosentritt et al., 2024a), which is why it cannot produce areal 3D information. Accuracy is further limited by the stylus

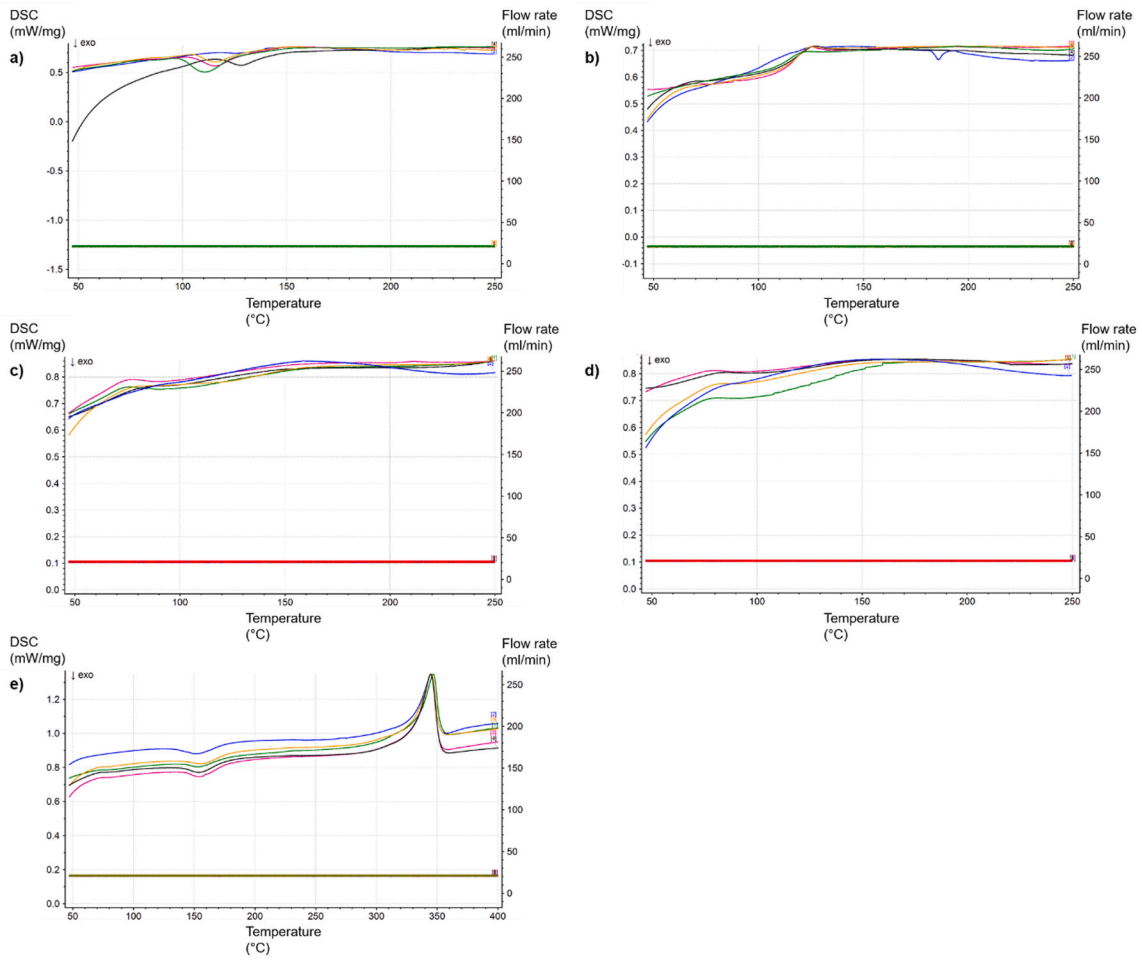

Fig. 8. Heat flow of denture base resin analyzed by differential scanning calorimetry. a) PMMA-C. b) PMMA-M. c) DMA90-P. d) DMA45-P. e) PEEK-M. The following line colours define the aging status: green: no aging. Blue: TC. Pink: TBA. Black: HCl. Orange: NaOCl. (For interpretation of the references to colour in this figure legend, the reader is referred to the Web version of this article.)

tip radius (typically ~2 μm); sensitive surfaces may be damaged (Mínguez-Martínez et al., 2022). However, due to differing measurement principles, both methods may yield different roughness values even for identical surfaces, with confocal systems generally reporting higher values (Rosentritt et al., 2024b). However, due to differing measurement principles, both methods may yield different roughness values even for similar surfaces, with confocal systems generally reporting higher values (Rosentritt et al., 2024a; Leach et al., 2014). The choice of magnification, depending on material and surface treatment, also affects the results (Rosentritt et al., 2024b).

Finally, from a clinical perspective, surface roughness is highly relevant. In some cases, R_a values exceeded the clinically relevant threshold for dental materials of 0.2 μm for bacterial adhesion following artificial aging (Schubert et al., 2019; Bollen et al., 1997). Additionally, patients can perceive surface changes with their tongue at thresholds as low as 0.3 μm (Jones et al., 2004), which may influence comfort and satisfaction. In the current study, smoother surfaces appeared to be less susceptible to age-related surface changes. This phenomenon could be attributed to a smaller surface area and fewer microstructural irregularities. Therefore, fine polishing of denture base materials is strongly recommended to minimize surface deterioration and ensure long-term clinical performance.

4.1.2. Surface free energy

TBA aging significantly increased SFE in PMMA-M and DMA45-P, while HCl and NaOCl storages caused relevant reductions in most materials except PEEK-M. PMMA-C and PMMA-M showed partial increases in SFE after storage in the various chemicals. Fine treatment generally led to higher SFE values higher after aging. TC induced the most pronounced alterations in SFE for all aging protocols, particularly in DMA90-P and DMA45-P, whereas PMMA-M and PEEK-M remained largely unaffected.

An increase in SFE following TC was also observed in conventionally fabricated PMMA (Hahnel et al., 2009). Zhang et al. (2024) reported that printed specimens showed higher distilled water contact angles and, thus, lower SFE compared to conventionally processed or milled materials, both before and after TC. This observation only partially relates to the results of the current study, which also showed a reduction in the SFE of the printed materials after TC. In agreement with a previous study, printed materials had higher SFE values compared to conventionally processed specimens, which then also showed a higher susceptibility to microbial colonization (Da Silva et al., 2023).

TC is a widely used method for simulating intraoral temperature fluctuations in artificial aging protocols. Alternating temperatures between 5 °C and 55 °C simulate thermal conditions in the oral cavity during the consumption of hot and cold foods or beverages and are commonly used in studies to evaluate thermal stress (Gad et al., 2022a; Gale and Darvell, 1999; Morresi et al., 2014; Bento et al., 2025). Assuming an average of 20–50 temperature fluctuations per day, a total of 10,000 thermal cycles is widely accepted as representing approximately one year of clinical use for removable dentures (Gale and Darvell, 1999; Bento et al., 2025). Repeated thermal stress may promote material

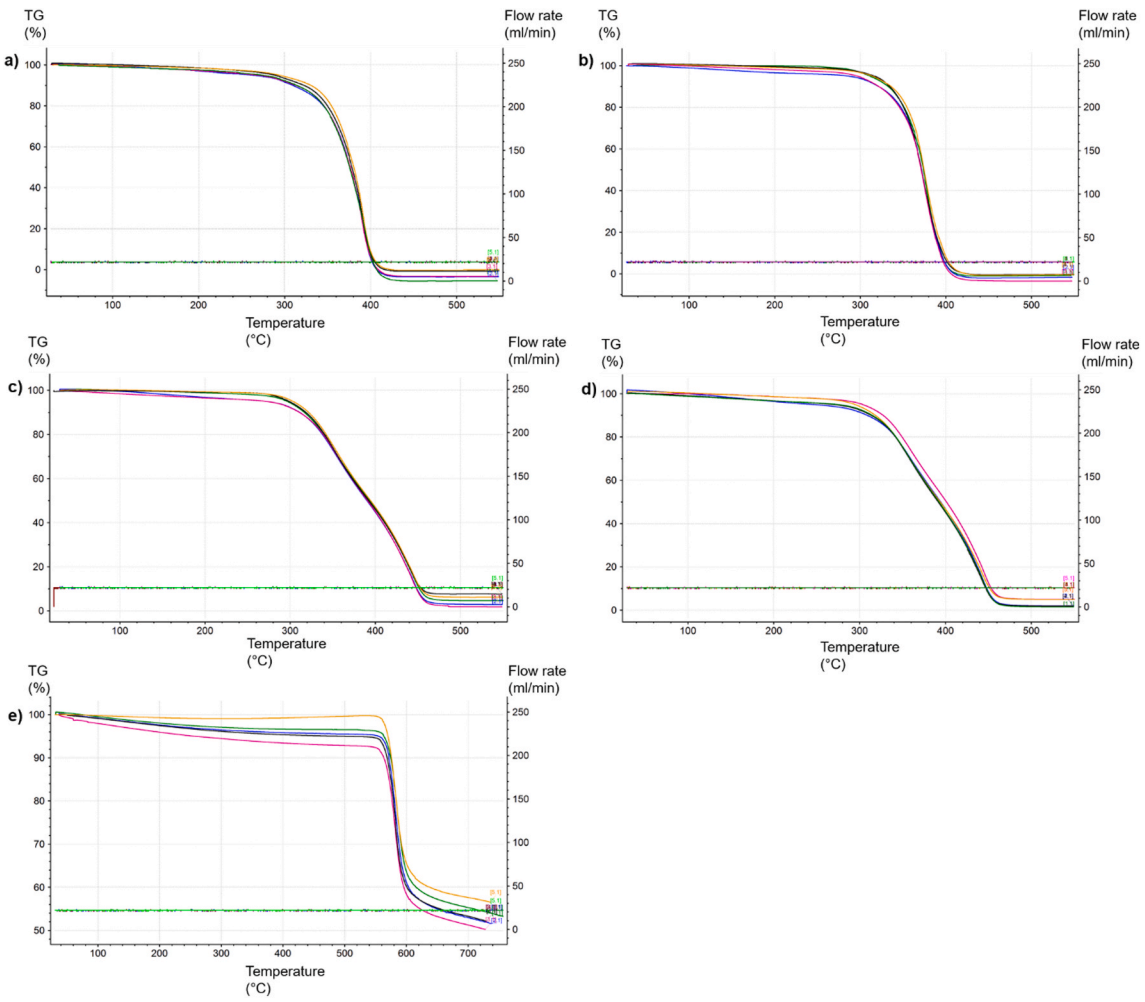

Fig. 9. Weight loss (%) of denture base resins analyzed by thermogravimetry. a) PMMA-C. b) PMMA-M. c) DMA90-P. d) DMA45-P. e) PEEK-M. The following line colours define the aging status: green: no aging. Blue: TC. Pink: TBA. Black: HCl. Orange: NaOCl. (For interpretation of the references to colour in this figure legend, the reader is referred to the Web version of this article.)

fatigue via water-induced microcracks, especially in polymers with high water absorption. Therefore, the TC protocol used in this study was chosen to simulate a clinically relevant long-term application under realistic intraoral conditions.

4.2. Microhardness and indentation

TC significantly reduced HM, H_{IT}, and E_{IT} in PMMA-C and PMMA-M, particularly after rough treatment. Other aging protocols had less impact, and DMA materials showed no relevant changes. PEEK-M exhibited the highest and most stable values across all parameters. Fine polishing slightly reduced hardness but also minimized aging effects.

Our findings partially contrast with those of Al-Dulaijan et al. (2022), who reported lower hardness in printed compared to heat-polymerized resins and who identified no influence of printing orientation. In the present study, reduced hardness was observed in printed specimens with a printing angle of 45°, suggesting orientation-specific effects. Similar to previous research (Porwal et al., 2017; Kurt et al., 2018), NaOCl led to a reduction in hardness in PMMA-based materials. However, pre-conditioning in water in those studies may have contributed to the outcome. The combination of different aging protocols likely intensified the degradation observed in the current results.

The negative influence of NaOCl on mechanical properties has been previously confirmed, with both heat-polymerized and printed DMA (100 μm layer thickness) showing decreased hardness after short-term immersion in 1 % NaOCl, especially with rougher surfaces (Elhagali et al., 2025). Atalay et al. (2021) also reported microhardness reduction after TC, and additional studies noted decreased hardness following water storage (Nguyen et al., 2017). In our study, PMMA-M showed a significant decline in hardness after all aging protocols, underlining its sensitivity to hydrothermal and chemical degradation.

A consistent relationship between Martens hardness and elastic modulus was identified, aligning with findings by Liebermann et al. (2016), who also reported correlated reductions in both parameters. While PEEK generally demonstrated high stability, a long-term NaOCl exposure (90 days) led to reductions in HM and E_{IT}, although initial resistance was high (Liebermann et al., 2016).

Surface and indentation hardness are crucial parameters for the durability of dental materials. They reflect resistance to deformation, wear, and scratching, factors directly impacting functional longevity under masticatory forces (Elhagali et al., 2025). The superior dimensional stability of PEEK, along with the orientation-dependent behaviour observed in printed DMA, highlights the critical role of material selection and processing in clinical applications. In particular, post-curing methods used on additively manufactured materials can have different effects on their mechanical properties and should be carefully considered when planning the workflow (Li et al., 2021). Fine polishing can further mitigate the effects of aging by reducing surface vulnerability.

4.3. Gravimetric determination of water absorption and solubility

TC significantly increased W_{sp} and W_{sl} in PMMA-M and DMA materials. PMMA-C remained largely unaffected, while PEEK-M consistently showed the lowest values across all conditions. Similar trends were identified after fine surface treatment, where the most pronounced effect was observed for DMA materials and the least for PEEK-M.

These results are in line with previous studies reporting the lowest sorption and solubility for PEEK compared to PMMA (Le Bars et al., 2023; Liebermann et al., 2016; Maloo et al., 2022). PMMA's higher polarity promotes water uptake (Atalay et al., 2021), which may explain its increased sensitivity. In printed materials, additional water absorption could be attributed to porosities introduced during the printing process, where air entrapment between layers creates microvoids (Gad et al., 2022a).

In particular, the DMA-based materials exhibited negative solubility values both before and after aging. Since solubility is calculated as the difference between the initial mass and the mass after storage, negative values occur when water uptake exceeds the actual material loss. This net mass gain may result from the chemical binding or physical retention of water molecules within the polymer matrix (Zhang et al., 2024; Nguyen et al., 2017).

However, negative solubility values do not exclude material loss. During water storage, sorption and leaching can occur simultaneously. If the material loss is overcompensated by higher water uptake, the calculated solubility becomes negative even though leaching or surface degradation may have taken place (Berli et al., 2020). Such processes can contribute to changes in surface topography, which is consistent with the roughness trends observed in the present study.

Although this study focused on surface-related parameters, aging-induced changes in microtopography are clinically relevant. Alterations in surface, mechanical, and sorptive properties can initiate cracks and promote stress concentration under functional loading. Previous research shows that water absorption, thermal fatigue, and related processes can soften the polymer matrix or create microdefects, thereby reducing the fracture resistance of denture base materials (Gad et al., 2022b; Izzettinoglu and Eroglu, 2025). Thus, the surface changes identified in this study may also suggest potential long-term effects on the structural integrity of PMMA-, DMA-, and PEEK-based materials. Clinically, high water sorption and solubility can impair dimensional stability and durability. The favourable behaviour of PEEK-M and the benefits of fine polishing suggest a more stable long-term performance under intraoral conditions.

4.4. Structural analyses

Thermal analyses enable the assessment of structural properties of polymeric materials, particularly glass transition, melting behaviour, and thermal stability (Meng et al., 2007; Kitagawa et al., 2020). The investigated materials differ in morphology: PMMA and the additively manufactured DMA specimens are predominantly amorphous, whereas PEEK, as a semi-crystalline high-performance polymer, comprises both crystalline and amorphous fractions. Crystalline domains remain structurally stable under moderate heating; consequently, materials with a crystalline fraction exhibit delayed softening and greater dimensional stability under thermal load compared with amorphous systems (Bargel and Schulze, 2008; Koltzenburg et al., 2024).

In PMMA-C and PMMA-M specimens, dominant reflexes could be seen across the amorphous region at 14.2 (111), 30.5 (112) and 42.1 (211), as also described here (Elashmawi and Hakeem, 2008; Sharma et al., 2023). Differences in the structure between printed and milled were not recognisable, at least by XRD.

According to the manufacturer, the two printed denture base materials DMA90-P and DMA45-P are based on a mixture of urethane and triethylene glycol dimethacrylate, among others. In contrast to PEEK-M, the XRD measurements show an X-ray amorphous composition (no remote order). The blurred large reflex at 17.8°/2θ and the two smaller blurred reflexes at 29.6°/2θ and 42.7°/2θ are confirmed by literature (Abu Bakar et al., 2022; Barszczewska-Rybarek, 2009; Balan et al., 2012).

As with PMMA, the crystallinity (crystalline fraction) of PEEK and, consequently, its final properties such as mechanical performance, translucency, and thermal or chemical resistance can be controlled by adjusting the processing temperature and cooling rate (Yang et al., 2017; Bassett et al., 1988; Lee et al., 2022). The crystalline content of approximately 25 % determined by XRD is corroborated by DSC analyses conducted by Yang et al. (2017), who demonstrated that increasing the temperature from 25 °C to 200 °C raised the degree of crystallinity from approximately 17 %–31 %.

The rutile phase (TiO_2) identified in PEEK-M acts as a white pigment due to its high reflectance of the visible light spectrum, thereby brightening the otherwise greyish PEEK (Soares Machado et al., 2022). However, the determined content (2 %) is insufficient to function as an effective UV blocker (≥5 %) (Bragaglia et al., 2020) or as a filler to enhance strength and hardness (10–30 %) (Soares Machado et al., 2022; Schmeiser et al., 2025; Micovic Soldatovic et al., 2022).

The lower proportion relative to the residual mass determined by TGA can be attributed to the small crystallite size (resolution limits of XRD) and the presence of additional components such as pigments (e.g. gingiva-colored additives). The reduction in TiO_2 particle size is particularly relevant, as it enhances the interfacial bonding between the filler and the polymer matrix, especially in combination with suitable silanes, and thereby improves the mechanical efficiency of the composite (Mishra et al., 2012; Kuo et al., 2005; Cazan et al., 2021).

Pigments could not be detected by XRD in any specimens, presumably due to the large amorphous proportion and low content.

In DSC, PMMA showed no melting transitions and a glass transition temperature around 100–110 °C. TC caused a flattened transition in PMMA-C, while PMMA-M showed an additional peak at ~190 °C under certain aging conditions, indicating higher sensitivity to aging than DMA and PEEK. No melting peak was observed for the DMA, reflecting the typical decomposition behaviour of highly crosslinked thermosets, which tends to decompose rather than melt (Bargel and Schulze, 2008; Rosentritt et al., 2018). Unchanged thermal profiles across all aging conditions and print orientations indicate a stable polymer network, in contrast to the orientation-dependent decomposition observed in TGA. PEEK exhibited a consistent and pronounced endothermic peak at approximately 340 °C across all conditions, corresponding to the melting point of its crystalline phase (Zanjanijam et al., 2020). The high melting temperature indicates a thermally robust crystalline structure. The stable DSC curves of DMA and PEEK indicate high thermal resilience, supporting their suitability for long-term clinical use under thermal and chemical stress.

TGA revealed the expected mass loss for all materials. Artificial aging produced no discernible changes in curve shape or residue, which indicates no detectable aging induced chemical modification. PMMA and DMA showed residues of 0 % for PMMA and near 0 % for DMA, consistent with the absence of inorganic fillers and with amorphous XRD signatures without additional crystalline reflexes. In contrast, PEEK exhibited a main degradation step at approximately 550–600 °C with a high residue of about 51–58 %, confirming the presence of an inorganic phase in agreement with the XRD diffraction pattern. In comparison, PMMA was thermally the least stable (conventional auto-curing < milled). DMA showed a medium level of stability with a decomposition onset that depended on the build angle (45° < 90°). PEEK displayed the highest thermal stability and the smallest aging induced changes.

In summary, the combined use of XRD, DSC, and TGA provided a consistent and complementary view of the structural and thermal characteristics of the examined denture base materials. The amorphous nature of PMMA- and DMA-based polymers was corroborated by the absence of distinct crystalline reflexes in XRD, the lack of melting transitions in DSC, and the nearly complete mass loss observed in TGA.

These materials exhibited low thermal stability and no indication of inorganic fillers. In contrast, the thermal and structural robustness of PEEK was confirmed by all three methods, highlighting its semi-crystalline composition, high-temperature transitions, and significant residual mass resulting from inorganic content. Altogether, these findings emphasize the critical role of material composition and processing technique in determining long-term performance under aging.

5. Conclusion

Based on the results of this study, and within the limitations of the study, the following conclusions can be drawn:

I. A finely polished surface significantly reduces the impact of aging processes on surface and material properties. The quality of surface treatment plays a decisive role in the aging resistance of denture base materials. From a clinical perspective, high-quality surface treatment is essential to ensure the long-term performance of RDPs.
II. The investigated materials exhibited distinct responses to aging processes. PMMA, as an established standard material for RDPs, showed aging-related changes depending on the manufacturing method. Milled PMMA demonstrated superior resistance to surface and mechanical degradation, making it a suitable alternative to both conventional auto-cured PMMA and additively processed DMA. Additively manufactured materials (DMA) displayed material- and orientation-dependent aging behaviour, with a build angle of 90° yielding the most favourable outcomes in terms of surface stability and mechanical performance. PEEK showed high structural stability across all aging protocols and thus presents a promising high-performance alternative to PMMA and DMA for long-term use in RDPs.
III. The selected manufacturing techniques significantly influences the surface and material properties. For both PMMA and PEEK, milling proves to be a high-quality and clinically alternative to the conventional auto-curing fabrication technique. Although additive manufacturing (printing) holds considerable potential, further research is required to improve material stability before it can be regarded as a clinically equivalent option for the fabrication of RDPs.

CRediT authorship contribution statement

Laura Brose: Writing – review & editing, Writing – original draft, Visualization, Validation, Methodology, Investigation, Formal analysis, Data curation, Conceptualization. **Andreas Koenig:** Writing – review & editing, Visualization, Validation, Investigation, Funding acquisition. **Paul Kemmesies:** Writing – review & editing, Visualization, Validation, Investigation. **Saba Tamjidtash:** Writing – review & editing. **Nadine Kommerein:** Writing – review & editing, Funding acquisition. **Katharina Doll-Nikutta:** Writing – review & editing. **Meike Stiesch:** Writing – review & editing. **Martin Rosentritt:** Writing – review & editing, Resources. **Sebastian Hahnel:** Writing – review & editing, Supervision, Funding acquisition, Conceptualization.

Funding

This work was funded by the Deutsche Forschungsgemeinschaft (DFG, German Research Foundation) - 470769735.

Declaration of competing interest

The authors declare that they have no known competing financial interests or personal relationships that could have appeared to influence the work reported in this paper.

Appendix A. Supplementary data

Supplementary data to this article can be found online at https://doi.org/10.1016/j.jmbbm.2025.107331.

Data availability

The datasets used in the current study are available from the corresponding author on reasonable request.

References

Abu Bakar, A.A., Zainuddin, M.Z., Abdullah, S.M., Tamchek, N., Mohd Noor, I.S., Alauddin, M.S., et al., 2022. The 3D printability and mechanical properties of polyhydroxybutyrate (PHB) as additives in urethane dimethacrylate (UDMA) blends polymer for medical application. Polymers. https://doi.org/10.3390/polym14214518.

Abuhajar, E., Ali, K., Zulfiqar, G., Al Ansari, K., Raja, H.Z., Bishti, S., Anweigi, L., 2023. Management of chronic atrophic candidiasis (Denture Stomatitis)-A narrative review. Int. J. Environ. Res. Publ. Health. https://doi.org/10.3390/ijerph20043029.

Al-Dulaijan, Y.A., Alsulaimi, L., Alotaibi, R., Alboainain, A., Alalawi, H., Alshehri, S., et al., 2022. Comparative evaluation of surface roughness and hardness of 3D printed resins. Materials. https://doi.org/10.3390/ma15196822.

Atalay, S., Çakmak, G., Fonseca, M., Schimmel, M., Yilmaz, B., 2021. Effect of thermocycling on the surface properties of CAD-CAM denture base materials after different surface treatments. J. Mech. Behav. Biomed. Mater. 121, 104646. https://doi.org/10.1016/j.jmbbm.2021.104646.

Babaier, R., Watts, D.C., Silikas, N., 2022. Effects of three food-simulating liquids on the roughness and hardness of CAD/CAM polymer composites. Dent. Mater. 38, 874–885. https://doi.org/10.1016/j.dental.2022.04.001.

Balan, L., Melinte, V., Buruiana, T., Schneider, R., Vidal, L., 2012. Controlling the morphology of gold nanoparticles synthesized photochemically in a polymer matrix through photonic parameters. Nanotechnology 23, 415705. https://doi.org/10.1088/0957-4484/23/41/415705.

Bargel, H.-J., Schulze, G., 2008. Werkstoffkunde. Springer Berlin Heidelberg, Berlin, Heidelberg.

Barszczewska-Rybarek, I.M., 2009. Structure-property relationships in dimethacrylate networks based on Bis-GMA, UDMA and TEGDMA. Dent. Mater. 25, 1082–1089. https://doi.org/10.1016/j.dental.2009.01.106.

Bassett, D.C., Olley, R.H., Ai Raheil, A.M., 1988. On crystallization phenomena in PEEK. Polymer 29, 1745–1754.

Bento, V.A.A., Sayeg, J.M.C., Del Rosa, C.D.R.D., Lopes, LFdTP., Marques, M.C.S., Pellizzer, E.P., 2025. Evaluation of optical, surface, and microbiological properties of computer-aided design/computer-aided manufacturing-milled and three-dimensional-printed denture bases after aging by thermocycling: an in vitro study. J. Indian Prosthodont. Soc. 25, 312–319. https://doi.org/10.4103/jips.jips_88_25.

Berli, C., Thieringer, F.M., Sharma, N., Müller, J.A., Dedem, P., Fischer, J., Rohr, N., 2020. Comparing the mechanical properties of pressed, milled, and 3D-printed resins for occlusal devices. J. Prosthet. Dent 124, 780–786. https://doi.org/10.1016/j.prosdent.2019.10.024.

Bollen, C., Lambrechts, P., Quirynen, M., 1997. Comparison of Surface Roughness of Oral Hard Materials to the Threshold Surface Roughness for Bacterial Plaque Retention: a Review of the Literature, vol. 13, pp. 258–269.

Bragaglia, M., Cherubini, V., Nanni, F., 2020. PEEK -TiO2 composites with enhanced UV resistance. Compos. Sci. Technol. 199, 108365. https://doi.org/10.1016/j.compscitech.2020.108365.

Brinkmann, L., Fuchs, F., Rosentritt, M., Schierz, O., Koenig, A., Reissmann, D.R., 2025. Effect of cleaning protocols on surface roughness of current polymeric denture materials. J. Forensic Biomech. 16, 359. https://doi.org/10.3390/jfb16100359.

Cazan, C., Enesca, A., Andronic, L., 2021. Synergic effect of TiO2 filler on the mechanical properties of polymer nanocomposites. Polymers. https://doi.org/10.3390/polym13122017.

Da Silva, M.D.D., Nunes, T.S.B.S., Viotto, HEdC., Coelho, S.R.G., Souza, RF de, Pero, A.C., 2023. Microbial adhesion and biofilm formation by Candida albicans on 3D-printed denture base resins. PLoS One 18, e0292430. https://doi.org/10.1371/journal.pone.0292430.

Dai, J., Spintzyk, S., Unkovskiy, A., Li, P., Xu, S., Kraemer Fernandez, P., 2022. Post-processing of DLP-printed denture base polymer: impact of a protective coating on the surface characteristics, flexural properties, cytotoxicity, and microbial adhesion. Dent. Mater. 38, 2062–2072. https://doi.org/10.1016/j.dental.2022.11.008.

Dimitrova, M., Vlahova, A., Hristov, I., Kazakova, R., 2024. Bonding efficiency between artificial teeth and denture base in CAD/CAM and conventional complete removable dentures. Materials. https://doi.org/10.3390/ma17133138.

Elashmawi, I.S., Hakeem, N.A., 2008. Effect of PMMA addition on characterization and morphology of PVDF. Polym. Eng. Sci. 48, 895–901. https://doi.org/10.1002/pen.21032.

Elhagali, A.F., Sharaf, M.Y., Abd El-Aziz, M.E.-S.A.A., Ali Bayiumy, A.S., Refaei, M.A.A., Al-Agamy, A.H., et al., 2025. The effects of different chemical disinfectants on the strength, surface, and color properties of conventional and 3D-Printed fabricated denture base materials. Prosthesis 7, 24. https://doi.org/10.3390/prosthesis7020024.

Gad, M.M., Fouda, S.M., Abualsaud, R., Alshahrani, F.A., Al-Thobity, A.M., Khan, S.Q., et al., 2022a. Strength and surface properties of a 3D-Printed denture base polymer. J. Prosthodont. 31, 412–418. https://doi.org/10.1111/jopr.13413.

Gad, M.M., Alshehri, S.Z., Alhamid, S.A., Albarrak, A., Khan, S.Q., Alshahrani, F.A., Alqarawi, F.K., 2022b. Water sorption, solubility, and translucency of 3D-Printed denture base resins. Dent. J. https://doi.org/10.3390/dj10030042.

Gale, M.S., Darvell, B.W., 1999. Thermal cycling procedures for laboratory testing of dental restorations. Jounal of Dentistry 27, 89–99.

Gendreau, L., Loewy, Z.G., 2011. Epidemiology and etiology of denture stomatitis. J. Prosthodont. 20, 251–260. https://doi.org/10.1111/j.1532-849X.2011.00698.x.

Gupta, A., Felton, D.A., Jemt, T., Koka, S., 2019. Rehabilitation of edentulism and mortality: a systematic review. J. Prosthodont. 28, 526–535. https://doi.org/10.1111/jopr.12792.

Hahnel, S., Rosentritt, M., Handel, G., Bürgers, R., 2009. In vitro evaluation of artificial ageing on surface properties and early Candida albicans adhesion to prosthetic resins. J. Mater. Sci. Mater. Med. 20, 249–255. https://doi.org/10.1007/s10856-008-3570-7.

Izzettinoglu, E., Eroglu, E., 2025. Assessing the impact of surface treatment, aging, and post-curing conditions on the water sorption and solubility of 3D-printed denture base resins compared to conventional and milled alternatives. BMC Oral Health 25, 1698. https://doi.org/10.1186/s12903-025-07115-7.

Jansen, D., Stabler, C., Goetz-Neunhoeffer, F., Dittrich, S., Neubauer, J., 2011. Does ordinary Portland cement contain amorphous phase? A quantitative study using an external standard method. Powder Diffr. 26, 31–38. https://doi.org/10.1154/1.3549186.

Jones, C.S., Billington, R.W., Pearson, G.J., 2004. The in vivo perception of roughness of restorations. Br. Dent. J. 196, 42–45. https://doi.org/10.1038/sj.bdj.4810881. ; discussion 31.

Kattadiyil, M.T., Jekki, R., Goodacre, C.J., Baba, N.Z., 2015. Comparison of treatment outcomes in digital and conventional complete removable dental prosthesis fabrications in a predoctoral setting. J. Prosthet. Dent 818–825.

Khangura, S.D., Grobelna, A., Haas, R., Subramonian, A., 2023. Longevity of partial and complete dentures. Canadian Journal of Health Technologies 3, 1–33.

Kitagawa, Y., Yoshida, K., Takase, K., Valanezhad, A., Watanabe, I., Kojio, K., Murata, H., 2020. Evaluation of viscoelastic properties, hardness, and glass transition temperature of soft denture liners and tissue conditioner. Odontology 108, 366–375. https://doi.org/10.1007/s10266-019-00477-9.

Koltzenburg, S., Maskos, M., Nuyken, O., 2024. Polymere: Synthese, Eigenschaften Und Anwendungen. Springer Berlin Heidelberg, Berlin, Heidelberg.

Kuo, M.C., Tsai, C.M., Huang, J.C., Chen, M., 2005. PEEK composites reinforced by nano-sized SiO2 and Al2O3 particulates. Mater. Chem. Phys. 90, 185–195. https://doi.org/10.1016/j.matchemphys.2004.10.009.

Kurt, A., Erkose-Genc, G., Uzun, M., Sarı, T., Isik-Ozkol, G., 2018. The effect of cleaning solutions on a denture base material: elimination of Candida albicans and alteration of physical properties. J. Prosthodont. 27, 577–583. https://doi.org/10.1111/jopr.12539.

Kurzendorfer, L., Schmidt, M., Hahnel, S., Rosentritt, M., 2023. Die digitale Prothesenfertigung. Quintessenz J. 49, 612–620.

Le Bars, P., Bandiaky, O.N., Le Guéhennec, L., Clouet, R., Kouadio, A.A., 2023. Different polymers for the base of removable dentures? Part I: a narrative review of mechanical and physical properties. Polymers. https://doi.org/10.3390/polym15173495.

Leach, R., Weckenmann, A., Coupland, J., Hartmann, W., 2014. Interpreting the probe-surface interaction of surface measuring instruments, or what is a surface? Surf. Topogr. Metrol. Prop. 2, 35001. https://doi.org/10.1088/2051-672X/2/3/035001.

Lee, D.J., Saponaro, P.C., 2019. Management of edentulous patients. Dent. Clin. 63, 249–261. https://doi.org/10.1016/j.cden.2018.11.006.

Lee, A., Wynn, M., Quigley, L., Salviato, M., Zobeiry, N., 2022. Effect of temperature history during additive manufacturing on crystalline morphology of PEEK. Advances in Industrial and Manufacturing Engineering 4, 100085. https://doi.org/10.1016/j.aime.2022.100085.

Lepišová, M., Tomášik, J., Oravcová, Ľ., Thurzo, A., 2025. Three-dimensional-printed elements based on polymer and composite materials in dentistry: a narrative review. Bratisl. Med. J. 126, 14–27. https://doi.org/10.1007/s44411-024-00011-6.

Li, P., Lambart, A.-L., Stawarczyk, B., Reymus, M., Spintzyk, S., 2021. Postpolymerization of a 3D-printed denture base polymer: impact of post-curing methods on surface characteristics, flexural strength, and cytotoxicity. J. Dent. 115, 103856. https://doi.org/10.1016/j.jdent.2021.103856.

Li, P., Kraemer Fernandez, P., Spintzyk, S., Schmidt, F., Yassine, J., Beuer, F., Unkovskiy, A., 2023. Effects of layer thickness and build angle on the microbial adhesion of denture base polymers manufactured by digital light processing. J Prosthodont Res 67, 562–567. https://doi.org/10.2186/jpr.JPR_D_22_00126.

Liebermann, A., Wimmer, T., Schmidlin, P.R., Scherer, H., Löffler, P., Roos, M., Stawarczyk, B., 2016. Physicomechanical characterization of polyetheretherketone and current esthetic dental CAD/CAM polymers after aging in different storage media. J. Prosthet. Dent 115, 321–328.

Lo Russo, L., Zhurakivska, K., Guida, L., Chochlidakis, K., Troiano, G., Ercoli, C., 2024. Comparative cost-analysis for removable complete dentures fabricated with conventional, partial, and complete digital workflows. J. Prosthet. Dent 131, 689–696.

Maloo, L.M., Toshniwal, S.H., Reche, A., Paul, P., Wanjari, M.B., 2022. A sneak peek toward polyaryletherketone (PAEK) polymer: a review. Cureus. https://doi.org/10.7759/cureus.31042.

Meng, F.H., Schricker, S.R., Brantley, W.A., Mendel, D.A., Rashid, R.G., Fields, H.W., et al., 2007. Differential scanning calorimetry (DSC) and temperature-modulated DSC study of three mouthguard materials. Dent. Mater. 23, 1492–1499. https://doi.org/10.1016/j.dental.2007.01.006.

Micovic Soldatovic, D., Liebermann, A., Huth, K.C., Stawarczyk, B., 2022. Fracture load of different veneered and implant-supported 4-UNIT cantilever PEEK fixed dental prostheses. J. Mech. Behav. Biomed. Mater. 129, 105173. https://doi.org/10.1016/j.jmbbm.2022.105173.

Mínguez-Martínez, A., Maresca, P., Caja, J., Oliva, JdVY., 2022. Results of a surface roughness comparison between stylus instruments and confocal microscopes. Materials. https://doi.org/10.3390/ma15165495.

Mishra, T.K., Kumar, A., Verma, V., Pandey, K.N., Kumar, V., 2012. PEEK composites reinforced with zirconia nanofiller. Compos. Sci. Technol. 72, 1627–1631. https://doi.org/10.1016/j.compscitech.2012.06.019.

Morresi, A.L., D'Amario, M., Capogreco, M., Gatto, R., Marzo, G., D'Arcangelo, C., Monaco, A., 2014. Thermal cycling for restorative materials: does a standardized protocol exist in laboratory testing? A literature review. J. Mech. Behav. Biomed. Mater. 29, 295–308. https://doi.org/10.1016/j.jmbbm.2013.09.013.

Muscat, Y., Farrugia, C., Camilleri, L., Arias-Moliz, M.T., Valdramidis, V., Camilleri, J., 2018. Investigation of acrylic resin disinfection using chemicals and ultrasound. J. Prosthodont. 27, 461–468. https://doi.org/10.1111/jopr.12511.

Nagar, P., Prasad, D.A., Satapathy, S.K., Vigneswaran, T., Francis, M., Vijaysingh, Jadhav A., 2024. Comparative study of conventional impressions vs intraoral scanning for complete denture fabrication. J. Pharm. BioAllied Sci. 16, S3746–S3748. https://doi.org/10.4103/jpbs.jpbs_1213_24.

Nguyen, L.G., Kopperud, H.M., Øilo, M., 2017. Water sorption and solubility of polyamide denture base materials. Acta Biomaterialia Odontologica Scandinavica. 3, 47–52. https://doi.org/10.1080/23337931.2017.1326009.

Owens, D.K., Wendt, R.C., 1969. Estimation of the surface free energy of polymers. J. Appl. Polym. Sci. 13, 1741–1747. https://doi.org/10.1002/app.1969.070130815.

Ozyilmaz, O.Y., Akin, C., 2019. Effect of cleansers on denture base resins' structural properties. J. Appl. Biomater. Funct. Mater. 17, 2280800019827797. https://doi.org/10.1177/2280800019827797.

Porwal, A., Khandelwal, M., Punia, V., Sharma, V., 2017. Effect of denture cleansers on color stability, surface roughness, and hardness of different denture base resins. J. Indian Prosthodont. Soc. 17, 61–67. https://doi.org/10.4103/0972-4052.197940.

Ribeiro, A.B., Tinelli, B.M., Clemente, L.M., Poker, BdC., Oliveira, VdC., Watanabe, E., Silva-Lovato, C.H., 2023. Effect of hygiene protocols on the mechanical and physical properties of two 3D-Printed denture resins characterized by extrinsic pigmentation as well as the mixed biofilm formed on the surface. Antibiotics (Basel). https://doi.org/10.3390/antibiotics12111630.

Roessler, D.M., 2003. Complete denture success for patients and dentists. Int. Dent. J. 53, 340–345. https://doi.org/10.1111/j.1875-595x.2003.tb00908.x.

Roos, E., Maile, K., 2015. Werkstoffkunde Für Ingenieure. Springer Berlin Heidelberg, Berlin, Heidelberg.

Rosentritt, M., 2018. Kunststoffe. In: Rosentritt, M., Ilie, N., Lohbauer, U. (Eds.), Werkstoffkunde in Der Zahnmedizin: Moderne Materialien Und Technologien. Georg Thieme Verlag, Stuttgart.

Rosentritt, M., Schneider-Feyrer, S., Kurzendorfer, L., 2024a. Comparison of surface roughness parameters Ra/Sa and Rz/Sz with different measuring devices. J. Mech. Behav. Biomed. Mater. 150, 106349. https://doi.org/10.1016/j.jmbbm.2023.106349.

Rosentritt, M., Schmutzler, A., Hahnel, S., Kurzendorfer-Brose, L., 2024b. The influence of CLSM magnification on the measured roughness of differently prepared dental materials. Materials. https://doi.org/10.3390/ma17235954.

Schmeiser, F., Schramm, W., Mayinger, F., Baumert, U., Stawarczyk, B., 2025. Effect of filler type, content, and silanization on the flexural strength, elastic modulus, shore D hardness, and two-body wear of PAEK compounds. Materials. https://doi.org/10.3390/ma18122736.

Schmohl, L., Roesner, A.J., Fuchs, F., Wagner, M., Schmidt, M.B., Hahnel, S., et al., 2022. Acid resistance of CAD/CAM resin composites. Biomedicines. https://doi.org/10.3390/biomedicines10061383.

Schmutzler, A., Rauch, A., Nitschke, I., Lethaus, B., Hahnel, S., 2021. Cleaning of removable dental protheses - a systematic review. J. Evid. Base Dent. Pract. 21, 1–12.

Schubert, A., Wassmann, T., Holtappels, M., Kurbad, O., Krohn, S., Bürgers, R., 2019. Predictability of microbial adhesion to dental materials by roughness parameters. Coatings 9, 456. https://doi.org/10.3390/coatings9070456.

Schwass, D.R., Lyons, K.M., Purton, D.G., 2013. How long will it last? The expected longevity of prosthodontic and restorative treatment. N. Z. Dent. J. 109, 98–105.

Sharma, S., Acharya, A.D., Bhawna, 2023. Fabrication of exfoliated BiOCl-Based PMMA nanocomposite with enhanced structural and thermal properties. Braz. J. Phys. https://doi.org/10.1007/s13538-023-01275-z.

Shim, J.S., Kim, J.-E., Jeong, S.H., Choi, Y.J., Ryu, J.J., 2020. Printing accuracy, mechanical properties, surface characteristics, and microbial adhesion of 3D-printed resins with various printing orientations. J. Prosthet. Dent 124, 468–475. https://doi.org/10.1016/j.prosdent.2019.05.034.

Soares Machado, P., Cadore Rodrigues, A.C., Chaves, E.T., Susin, A.H., Valandro, L.F., Pereira, G.K.R., Rippe, M.P., 2022. Surface treatments and adhesives used to increase the bond strength between polyetheretherketone and resin-based dental materials: a scoping review. J. Adhesive Dent. 24, 233–245. https://doi.org/10.3290/j.jad.b2288283.

Taylor, M., Masood, M., Mnatzaganian, G., 2021. Longevity of complete dentures: a systematic review and meta-analysis. J. Prosthet. Dent 125, 611–619.

Tieh, M.T., Waddell, J.N., Choi, J.J.E., 2022. Optical and mechanical properties of conventional, milled and 3D-printed denture teeth. J. Mech. Behav. Biomed. Mater. 126, 105061. https://doi.org/10.1016/j.jmbbm.2021.105061.

Wang, C., Shi, Y.-F., Xie, P.-J., Wu, J.-H., 2021. Accuracy of digital complete dentures: a systematic review of in vitro studies. J. Prosthet. Dent 125, 249–256. https://doi.org/10.1016/j.prosdent.2020.01.004.

Yang, C., Tian, X., Li, D., Cao, Y., Zhao, F., Shi, C., 2017. Influence of thermal processing conditions in 3D printing on the crystallinity and mechanical properties of PEEK material. J. Mater. Process. Technol. 248, 1–7. https://doi.org/10.1016/j.jmatprotec.2017.04.027.

Zanjanijam, A.R., Major, I., Lyons, J.G., Lafont, U., Devine, D.M., 2020. Fused filament fabrication of PEEK: a review of process-structure-property relationships. Polymers. https://doi.org/10.3390/polym12081665.

Zhang, R.-J., Zhao, L., Yu, L.-X., Tan, F.-B., 2024. Influence of thermal-cycling or staining medium on the surface properties and color stability of conventional, milled, and 3D-printed base materials. Sci. Rep. 14, 28928. https://doi.org/10.1038/s41598-024-80380-8.